What Geometric Visual Hallucinations Tell Us about the Visual Cortex

Paul C. Bressloff
bressloff@math.utah.edu
Department of Mathematics, University of Utah, Salt Lake City, Utah 84112, U.S.A.

Jack D. Cowan
cowan@math.uchicago.edu
Department of Mathematics, University of Chicago, Chicago, IL 60637, U.S.A.

Martin Golubitsky
mg@math.uh.edu
Department of Mathematics, University of Houston, Houston, TX 77204-3476, U.S.A.

Peter J. Thomas
pjthomas@salk.edu
Computational Neurobiology Laboratory, Salk Institute for Biological Studies, San Diego, CA 92186-5800, U.S.A.

Matthew C. Wiener
mcw@ln.nimh.nih.gov
Laboratory of Neuropsychology, National Institutes of Health, Bethesda, MD 20892, U.S.A.

Many observers see geometric visual hallucinations after taking hallucinogens such as LSD, cannabis, mescaline or psilocybin; on viewing bright flickering lights; on waking up or falling asleep; in "near-death" experiences; and in many other syndromes. Klüver organized the images into four groups called *form constants*: (I) tunnels and funnels, (II) spirals, (III) lattices, including honeycombs and triangles, and (IV) cobwebs. In most cases, the images are seen in both eyes and move with them. We interpret this to mean that they are generated in the brain. Here, we summarize a theory of their origin in visual cortex (area V1), based on the assumption that the form of the retino–cortical map and the architecture of V1 determine their geometry. (A much longer and more detailed mathematical version has been published in *Philosophical Transactions of the Royal Society B, 356* [2001].)

We model V1 as the continuum limit of a lattice of interconnected hypercolumns, each comprising a number of interconnected iso-orientation columns. Based on anatomical evidence, we assume that the lateral con-

nectivity between hypercolumns exhibits symmetries, rendering it invariant under the action of the Euclidean group $E(2)$, composed of reflections and translations in the plane, and a (novel) shift-twist action. Using this symmetry, we show that the various patterns of activity that spontaneously emerge when V1's spatially uniform resting state becomes unstable correspond to the form constants when transformed to the visual field using the retino-cortical map. The results are sensitive to the detailed specification of the lateral connectivity and suggest that the cortical mechanisms that generate geometric visual hallucinations are closely related to those used to process edges, contours, surfaces, and textures.

1 Introduction

Seeing vivid visual hallucinations is an experience described in almost all human cultures. Painted hallucinatory images are found in prehistoric caves (Clottes & Lewis-Williams, 1998) and scratched on petroglyphs (Patterson, 1992). Hallucinatory images are seen both when falling asleep (Dybowski, 1939) and on waking up (Mavromatis, 1987), following sensory deprivation (Zubek, 1969), after taking ketamine and related anesthetics (Collier, 1972), after seeing bright flickering light (Purkinje, 1918; Helmholtz, 1925; Smythies, 1960), or on applying deep binocular pressure on the eyeballs (Tyler, 1978), in "near-death" experiences (Blackmore, 1992), and, most striking, shortly after taking hallucinogens containing ingredients such as LSD, cannabis, mescaline, or psilocybin (Siegel & Jarvik, 1975). In most cases, the images are seen in both eyes and move with them, but maintain their relative positions in the visual field. We interpret this to mean that they are generated in the brain. One possible location for their origin is provided by fMRI studies of visual imagery suggesting that V1 is activated when human subjects are instructed to inspect the fine details of an imagined visual object (Miyashita, 1995). In 1928, Klüver (1966) organized such images into four groups called *form constants*: (I) tunnels and funnels, (II) spirals, (III) lattices, including honeycombs and triangles, and (IV) cobwebs, all of which contain repeated geometric structures. Figure 1 shows their appearance in the visual field. Ermentrout and Cowan (1979) provided a first account of a theory of the generation of such form constants. Here we develop and elaborate this theory in the light of the anatomical and physiological data that have accumulated since then.

1.1 Form Constants and the Retino–Cortical Map. Assuming that form constants are generated in part in V1, the first step in constructing a theory of their origin is to compute their appearance in V1 coordinates. This is done using the topographic map between the visual field and V1. It is well established that the central region of the visual field has a much bigger representation in V1 than does the peripheral field (Drasdo, 1977; Sereno

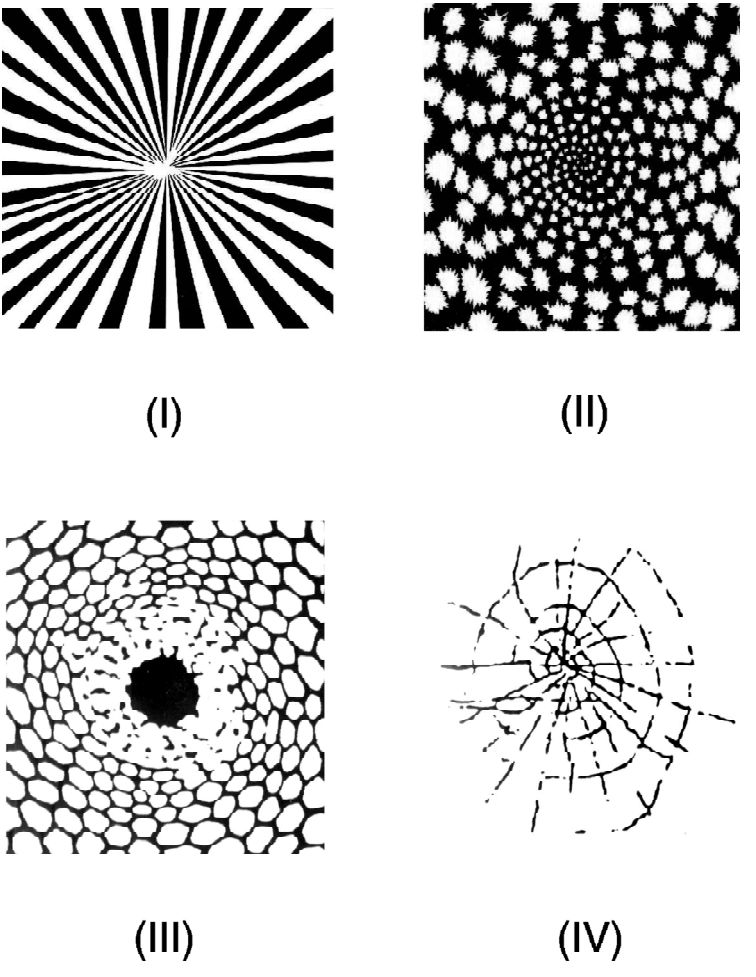

Figure 1: Hallucinatory form constants. (I) Funnel and (II) spiral images seen following ingestion of LSD (redrawn from Siegel & Jarvik, 1975), (III) honeycomb generated by marijuana (redrawn from Siegel & Jarvik, 1975), and (IV) cobweb petroglyph (redrawn from Patterson, 1992).

et al., 1995). Such a nonuniform retino-cortical magnification is generated by the nonuniform packing density of ganglion cells in the retina, whose axons in the optic nerve target neurons in the lateral geniculate nucleus (LGN), and (subsequently) in V1, that are much more uniformly packed. Let $\mathbf{r}_R = \{r_R, \theta_R\}$ be the (polar) coordinates of a point in the visual field and $\mathbf{r} = \{x, y\}$ its corresponding V1 coordinates. Given a retinal ganglion cell

packing density ρ_R (cells per unit retinal area) approximated by the inverse square law,

$$\rho_R = \frac{1}{(w_0 + \epsilon r_R)^2},$$

(Drasdo, 1977), and a uniform V1 packing density ρ, we derive a coordinate transformation (Cowan, 1977) that reduces, sufficiently far away from the fovea (when $r_R \gg w_0/\epsilon$) to a scaled version of the complex logarithm (Schwartz, 1977),

$$x = \frac{\alpha}{\epsilon} \ln\left[\frac{\epsilon}{w_0} r_R\right], \qquad y = \frac{\beta \theta_R}{\epsilon}, \tag{1.1}$$

where w_0 and ϵ are constants. Estimates of $w_0 = 0.087$ and $\epsilon = 0.051$ in appropriate units can be obtained from Drasdo's data on the human retina, and α and β are constants. These values correspond to a magnification factor of 11.5 mm/degrees of visual angle at the fovea and 5.75 mm/degrees of visual angle at $r_R = w_0/\epsilon = 1.7$ degrees of visual angle. We can also compute how the complex logarithm maps local edges or contours in the visual field, that is, its tangent map. Let ϕ_R be the orientation preference of a neuron in V1 whose receptive field is centered at the point $\mathbf{r}_R$ in the visual field, and let $\{\mathbf{r}, \phi\}$ be the V1 image of $\{\mathbf{r}_R, \phi_R\}$. It can be shown (Wiener, 1994; Cowan, 1997; Bressloff, Cowan, Golubitsky, Thomas, & Wiener, 2001) that under the tangent map of the complex logarithm, $\phi = \phi_R - \theta_R$. Given the retino-cortical map $\{\mathbf{r}_R, \phi_R\} \to \{\mathbf{r}, \phi\}$, we can compute the form of logarithmic spirals, circles, and rays and their local tangents in V1 coordinates. The equation for spirals can be written as $\theta_R = a \ln[r_R \exp(-b)] + c$, whence $y - c = a(x - b)$ under the action $\mathbf{r}_R \to \mathbf{r}$. Thus, logarithmic spirals become oblique lines of constant slope a in V1. Circles and rays correspond to vertical ($a = \infty$) and horizontal ($a = 0$) lines. Since the slopes of the local tangents to logarithmic spirals are given by the equation $\tan(\phi_R - \theta_R) = a$, and therefore in V1 coordinates by $\tan\phi = a$, the local tangents in V1 lie parallel to the images of logarithmic spirals. It follows that types I and II form constants corresponding to stripes of neural activity at various angles in V1 and types III and IV to spatially periodic patterns of local tangents in V1, as shown in Figure 2. On the average, about 30 to 36 stripes and about 60 to 72 contours are perceived in the visual field, corresponding to a wavelength of about 2.4 to 3.2 mm in human V1. This is comparable to estimates of about twice V1 hypercolumn spacing (Hubel & Wiesel, 1974) derived from the responses of human subjects to perceived grating patterns (Tyler, 1982) and from direct anatomical measurements of human V1 (Horton & Hedley-Whyte, 1984). All of these facts and calculations reinforce the suggestion that the form constants are located in V1. It might be argued that since hallucinatory images are seen as continuous across the midline, they must be located at higher levels in the visual pathway than V1. However,

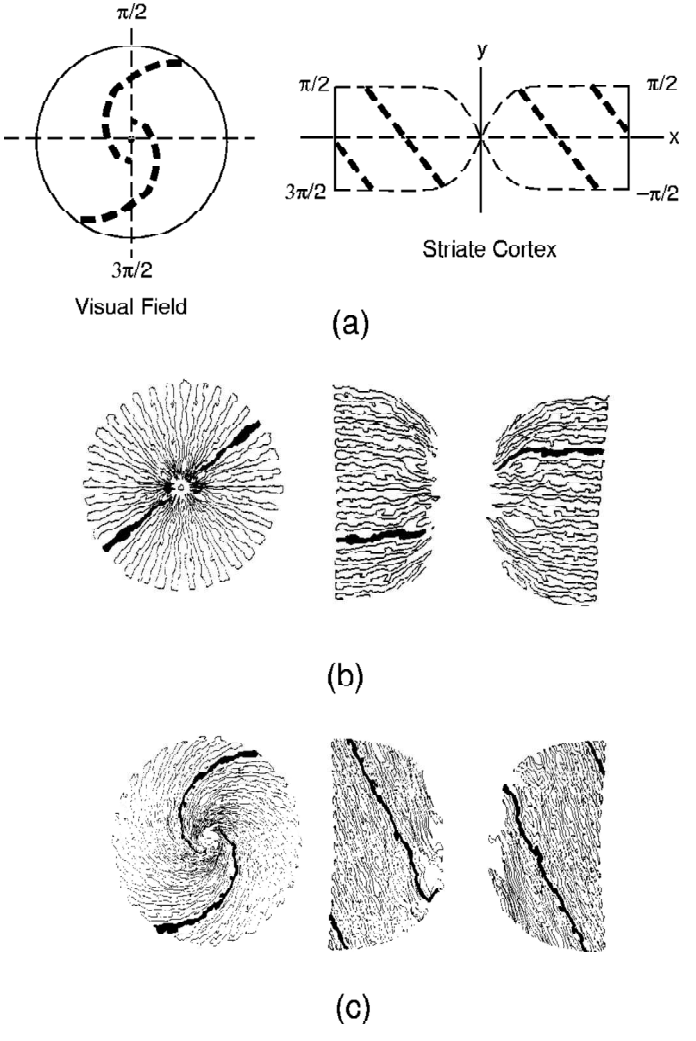

Figure 2: (a) Retino-cortical transform. Logarithmic spirals in the visual field map to straight lines in V1. (b, c) The action of the map on the outlines of funnel and spiral form constants.

there is evidence that callosal connections along the V1/V2 border can act to maintain continuity of the images across the vertical meridian (Hubel & Wiesel, 1962). Thus, if hallucinatory images are generated in both halves of V1, as long as the callosal connections operate, such images will be continuous across the midline.

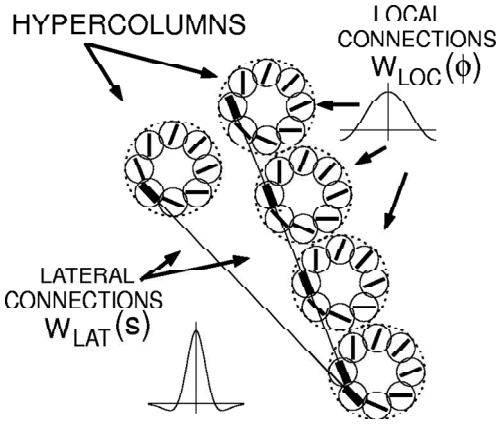

Figure 3: Outline of the architecture of V1 represented by equation 1.2. Local connections between iso-orientation patches within a hypercolumn are assumed to be isotropic. Lateral connections between iso-orientation patches in different hypercolumns are assumed to be anisotropic.

1.2 Symmetries of V1 Intrinsic Circuitry. In recent years, data concerning the functional organization and circuitry of V1 have accrued from microelectrode studies (Gilbert & Wiesel, 1983), labeling, and optical imaging (Blasdel & Salama, 1986; Bosking, Zhang, Schofield, & Fitzpatrick, 1997). Perhaps the most striking result is Blasdel and Salama's (1986) demonstration of the large-scale organization of iso-orientation patches in primates. We can conclude that approximately every 0.7 mm or so in V1 (in macaque), there is an iso-orientation patch of a given preference ϕ and that each hypercolumn has a full complement of such patches, with preferences running from ϕ to $\phi + \pi$. The other striking result concerns the intrinsic horizontal connections in layers 2, 3, and (to some extent) 5 of V1. The axons of these connections make terminal arbors only every 0.7 mm or so along their tracks (Gilbert & Wiesel, 1983), and connect mainly to cells with similar orientation preferences (Bosking et al., 1997). In addition, there is a pronounced anisotropy to the pattern of such connections: differing iso-orientation patches preferentially connect to patches in neighboring hypercolumns in such a way as to form continuous contours under the action of the retino-cortical map described above (Gilbert & Wiesel, 1983; Bosking et al., 1997). This contrasts with the pattern of connectivity within any one hypercolumn, which is much more isotropic: any given iso-orientation patch connects locally in all directions to all neighboring patches within a radius of less than 0.7 mm (Blasdel & Salama, 1986). Figure 3 shows a diagram of such connection patterns.

Since each location in the visual field is represented in V1, roughly speaking, by a hypercolumn-sized region containing all orientations, we treat $\mathbf{r}$ and ϕ as independent variables, so that all possible orientation preferences exist at each corresponding position $\mathbf{r}_R$ in the visual field. This continuum approximation allows a mathematically tractable treatment of V1 as a lattice of hypercolumns. Because the actual hypercolumn spacing (Hubel & Wiesel, 1974) is about half the effective cortical wavelength of many of the images we wish to study, care must be taken in interpreting cortical activity patterns as visual percepts. In addition, it is possible that lattice effects could introduce deviations from the continuum model. Within the continuum framework, let $w(\mathbf{r}, \phi \mid \mathbf{r}', \phi')$ be the strength or weight of connections from the iso-orientation patch at $\{x', y'\} = \mathbf{r}'$ in V1 with orientation preference ϕ' to the patch at $\{x, y\} = \mathbf{r}$ with preference ϕ. We decompose w in terms of local connections from elements within the same hypercolumn and patchy lateral connections from elements in other hypercolumns, that is,

$$w(\mathbf{r}, \phi \mid \mathbf{r}', \phi') = w_{LOC}(\phi - \phi')\delta(\mathbf{r} - \mathbf{r}') + \beta w_{LAT}(s)\delta(\mathbf{r} - \mathbf{r}' - s\mathbf{e}_\phi)\delta(\phi - \phi'), \tag{1.2}$$

where $\delta(\cdot)$ is the Dirac delta function, $\mathbf{e}_\phi$ is a unit vector in the ϕ–direction, β is a parameter that measures the weight of lateral relative to local connections, and $w_{LAT}(s)$ is the weight of lateral connections between iso-orientation patches separated by a cortical distance s along a visuotopic axis parallel to their orientation preference. The fact that the lateral weight depends on a rotated vector expresses its anisotropy. Observations by Hirsch and Gilbert (1991) suggest that β is small and therefore that the lateral connections modulate rather than drive V1 activity. It can be shown (Wiener, 1994; Cowan, 1997; Bressloff et al., 2001) that the weighting function defined in equation 1.2 has a well-defined symmetry: it is invariant with respect to certain operations in the plane of V1–translations $\{\mathbf{r}, \phi\} \to \{\mathbf{r} + \mathbf{u}, \phi\}$, reflections $\{x, y, \phi\} \to \{x, -y, -\phi\}$, and a rotation defined as $\{\mathbf{r}, \phi\} \to \{R_\theta[\mathbf{r}], \phi + \theta\}$, where $R_\theta[\mathbf{r}]$ is the vector $\mathbf{r}$ rotated by the angle θ. This form of the rotation operation follows from the anisotropy of the lateral weighting function and comprises a translation or shift of the orientation preference label ϕ to $\phi + \theta$, together with a rotation or twist of the position vector $\mathbf{r}$ by the angle θ. Such a shift-twist operation (Zweck & Williams, 2001) provides a novel way to generate the Euclidean group $E(2)$ of rigid motions in the plane. The fact that the weighting function is invariant with respect to this form of $E(2)$ has important consequences for any model of the dynamics of V1. In particular, the equivariant branching lemma (Golubitsky & Schaeffer, 1985) guarantees that when the homogeneous state $a(\mathbf{r}, \phi) = 0$ becomes unstable, new states with the symmetry of certain subgroups of $E(2)$ can arise. These new states will be linear combinations of patterns we call *planforms*.

2 A Model of the Dynamics of V1

Let $a(\mathbf{r}, \phi, t)$ be the average membrane potential or activity in an iso-orientation patch at the point $\mathbf{r}$ with orientation preference ϕ. The activity variable $a(\mathbf{r}, \phi, t)$ evolves according to a generalization of the Wilson-Cowan equations (Wilson & Cowan, 1973) that incorporates an additional degree of freedom to represent orientation preference and the continuum limit of the weighting function defined in equation 1.2:

$$\frac{\partial a(\mathbf{r}, \phi, t)}{\partial t} = -\alpha a(\mathbf{r}, \phi, t) + \frac{\mu}{\pi} \int_0^\pi w_{LOC}(\phi - \phi')\sigma[a(\mathbf{r}, \phi', t)]d\phi' + \nu \int_{-\infty}^{\infty} w_{LAT}(s)\sigma[a(\mathbf{r} + s\mathbf{e}_\phi, \phi, t)]\, ds, \tag{2.1}$$

where α, μ, and $\nu = \mu\beta$ are, respectively, time and coupling constants, and $\sigma[a]$ is a smooth sigmoidal function of the activity a. It remains only to specify the form of the functions $w_{LOC}(\phi)$ and $w_{LAT}(s)$. In the single population model considered here, we do not distinguish between excitatory and inhibitory neurons and therefore assume both $w_{LOC}(\phi)$ and $w_{LAT}(s)$ to be "Mexican hats" of the generic form,

$$\sigma_1^{-1} \exp(-x^2/2\sigma_1^2) - \sigma_2^{-1} \exp(-x^2/2\sigma_2^2), \tag{2.2}$$

with Fourier transform

$$W(p) = \exp(-\sigma_1^2 p^2) - \exp(-\sigma_2^2 p^2),$$

$(\sigma_1 < \sigma_2)$, such that iso-orientation patches at nearby locations mutually excite if they have similar orientation preferences, and inhibit otherwise, and similar iso-orientation patches at locations at least $\mathbf{r}_0$ mm apart mutually inhibit. In models that distinguish between excitatory and inhibitory populations, it is possible to achieve similar results using inverted Mexican hat functions that incorporate short-range inhibition and long-range excitation. Such models may provide a better fit to anatomical data (Levitt, Lund, & Yoshioka, 1996).

An equation $F[a] = 0$ is said to be equivariant with respect to a symmetry operator γ if it commutes with it, that is, if $\gamma F[a] = F[\gamma a]$. It follows from the Euclidean symmetry of the weighting function $w(\mathbf{r}, \phi \mid \mathbf{r}', \phi')$ with respect to the shift-twist action that equation 2.1 is equivariant with respect to it. This has important implications for the dynamics of our model of V1. Let $a(\mathbf{r}, \phi) = 0$ be a homogeneous stationary state of equation 2.1 that depends smoothly on the coupling parameter μ. When no iso-orientation patches are activated, it is easy to show that $a(\mathbf{r}, \phi) = 0$ is stable for all values of μ less than a critical value μ_0 (Ermentrout, 1998). However, the parameter μ can reach μ_0 if, for example, the excitability of V1 is increased by the action of hallucinogens on brain stem nuclei such as the locus ceruleus or the

raphe nucleus, which secrete the monoamines serotonin and noradrenalin. In such a case, the homogeneous stationary state $a(\mathbf{r}, \phi) = 0$ becomes unstable. If μ remains close to μ_0, then new stationary states develop that are approximated by (finite) linear combinations of the eigenfunctions of the linearized version of equation 2.1. The equivariant branching lemma (Golubitsky & Schaeffer, 1985) then guarantees the existence of new states with the symmetry of certain subgroups of the Euclidean group $E(2)$. This mechanism, by which dynamical systems with Mexican hat interactions can generate spatially periodic patterns that displace a homogeneous equilibrium, was first introduced by Turing (1952) in his article on the chemical basis of morphogenesis.

2.1 Eigenfunctions of V1. Computing the eigenvalues and associated eigenfunctions of the linearized version of equation 2.1 is nontrivial, largely because of the presence of the anisotropic lateral connections. However, given that lateral effects are only modulatory, so that $\beta \ll 1$, degenerate Rayleigh-Schrödinger perturbation theory can be used to compute them (Bressloff et al., 2001). The results can be summarized as follows. Let σ_1 be the slope of $\sigma[a]$ at the stationary equilibrium $a = 0$. Then to lowest order in β, the eigenvalues $\lambda_\pm$ are

$$\lambda_\pm(p, q) = -\alpha + \mu\sigma_1[W_{LOC}(p) + \beta\{W_{LAT}(0, q) \pm W_{LAT}(2p, q)\}], \quad (2.3)$$

where $W_{LOC}(p)$ is the pth Fourier mode of $w_{LOC}(\phi)$ and

$$W_{LAT}(p, q) = (-1)^p \int_0^\infty w_{LAT}(s) J_{2p}(qs)\, ds$$

is the Fourier transform of the lateral weight distribution with $J_{2p}(x)$ the Bessel function of x of integer order $2p$. To these eigenvalues belong the associated eigenfunctions

$$\begin{aligned} \nu^\pm(\mathbf{r}, \phi) = {} & c_n u^\pm(\phi - \phi_n) exp[i\mathbf{k}_n \cdot \mathbf{r}] \\ & + c_n^* u^{\pm *}(\phi - \phi_n) exp[-i\mathbf{k}_n \cdot \mathbf{r}], \end{aligned} \quad (2.4)$$

where $\mathbf{k}_n = \{q \cos\phi_n, q \sin\phi_n\}$ and (to lowest order in β), $u^\pm(\phi) = \cos 2p\phi$ or $\sin 2p\phi$, and the $*$ operator is complex conjugation. These functions will be recognized as plane waves modulated by even or odd phase-shifted π–periodic functions $\cos[2p(\phi - \phi_n)]$ or $\sin[2p(\phi - \phi_n)]$. The relation between the eigenvalues $\lambda_\pm$ and the wave numbers p and q given in equation 2.3 is called a *dispersion relation*. In case $\lambda_\pm = 0$ at $\mu = \mu_0$, equation 2.3 can be rewritten as

$$\mu_c = \frac{\alpha}{\sigma_1[W_{LOC}(p) + \beta\{W_{LAT}(0, q) + W_{LAT}(2p, q)\}]} \quad (2.5)$$

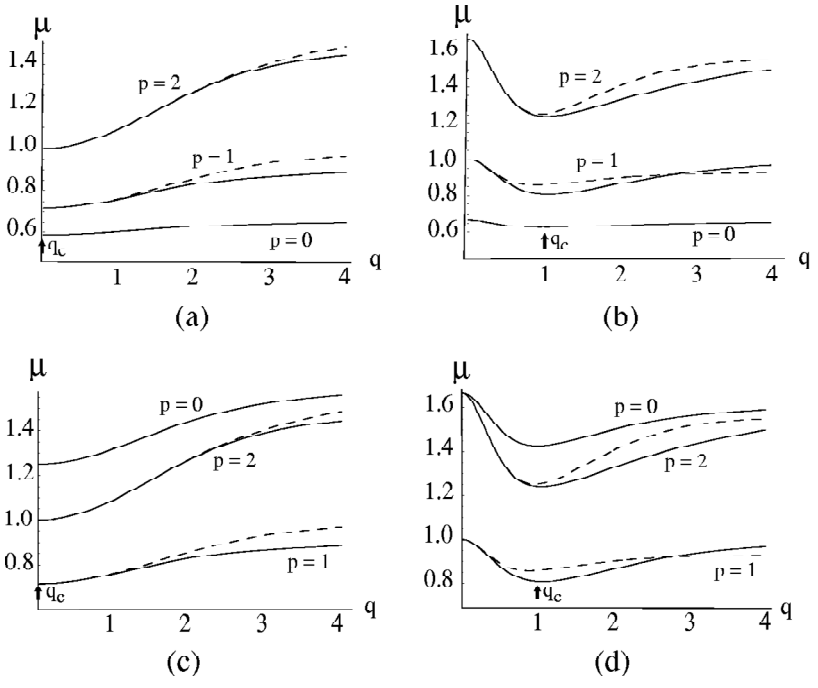

Figure 4: Dispersion curves showing the marginal stability of the homogeneous mode of V1. Solid lines correspond to odd eigenfunctions, dashed lines to even ones. If V1 is in the Hubel-Wiesel mode ($p_c = 0$), eigenfunctions in the form of unmodulated plane waves or roll patterns can appear first at the wave numbers (a) $q_c = 0$ and (b) $q_c = 1$. If V1 is in the coupled–ring mode ($p_c = 1$), odd modulated eigenfunctions can form first at the wave numbers (c) $q_c = 0$ and (d) $q_c = 1$.

and gives rise to the marginal stability curves plotted in Figure 4. Examination of these curves indicates that the homogeneous state $a(\mathbf{r}, \phi) = 0$ can lose its stability in four differing ways, as shown in Table 1.

Table 1: Instabilities of V1.

Wave Numbers	Local Interactions	Lateral Interactions	Eigenfunction
$p_c = q_c = 0$	Excitatory	Excitatory	c_n
$p_c = 0, q_c \neq 0$	Excitatory	Mexican hat	$c_n \cos[\mathbf{k}_n \cdot \mathbf{r}]$
$p_c \neq 0, q_c = 0$	Mexican hat	Excitatory	$c_n u^{\pm}(\phi - \phi_n) + c_n^* u^{\pm *}(\phi - \phi_n)$
$p_c \neq 0, q_c \neq 0$	Mexican hat	Mexican hat	$c_n u^{\pm}(\phi - \phi_n) \cos[\mathbf{k}_n \cdot \mathbf{r}]$

We call responses with $p_c = 0$ (rows 1 and 2) the *Hubel-Wiesel mode* of V1 operation. In such a mode, any orientation tuning must be extrinsic to V1, generated, for example, by local anisotropies of the geniculo-cortical map (Hubel & Wiesel, 1962). We call responses with $p_c \neq 0$ (rows 3 and 4) the *coupled ring mode* of V1 operation (Somers, Nelson, & Sur, 1996; Hansel & Sompolinsky, 1997; Mundel, Dimitrov, & Cowan, 1997). In both cases, the model reduces to a system of coupled hypercolumns, each modeled as a ring of interacting iso-orientation patches with local excitation and inhibition. Even if the lateral interactions are weak ($\beta \ll 1$), the orientation preferences become spatially organized in a pattern given by some combination of the eigenfunctions $\nu^{\pm}(\mathbf{r}, \phi)$.

3 Planforms and V1

It remains to compute the actual patterns of V1 activity that develop when the uniform state loses stability. These patterns will be linear combinations of the eigenfunctions described above, which we call *planforms*. To compute them, we find those planforms that are left invariant by the axial subgroups of $E(2)$ under the shift-twist action. An axial subgroup is a restricted set of the symmetry operators of a group, whose action leaves invariant a one-dimensional vector subspace containing essentially one planform. We limit these planforms to regular tilings of the plane (Golubitsky, Stewart, & Schaeffer, 1988), by restricting our computation to doubly periodic planforms. Given such a restriction, there are only a finite number of shift-twists to consider (modulo an arbitrary rotation of the whole plane), and the axial subgroups and their planforms have either rhombic, square, or hexagonal symmetry. To determine which planforms are stabilized by the nonlinearities of the system, we use Lyapunov-Schmidt reduction (Golubitsky et al., 1988) and Poincaré-Lindstedt perturbation theory (Walgraef, 1997) to reduce the dynamics to a set of nonlinear equations for the amplitudes c_n in equation 2.4. Euclidean symmetry restricts the structure of the amplitude equations to the form (on rhombic and square lattices)

$$\frac{d}{dt}c_n = c_n[(\mu - \mu_0) - \gamma_0|c_n|^2 - 2\sum_{m\neq n}^{2}\gamma_{nm}|c_m|^2], \tag{3.1}$$

where γ_{nm} depends on $\Delta\phi$, the angle between the two eigenvectors of the lattice. We find that all rhombic planforms with $30^\circ \leq \Delta\phi \leq 60^\circ$ are stable. Similar equations obtain for hexagonal lattices. In general, all such planforms on rhombic and hexagonal lattices are stable (in appropriate parameter regimes) with respect to perturbations with the same lattice structure. However, square planforms on square lattices are unstable and give way to simple roll planforms comprising one eigenfunction.

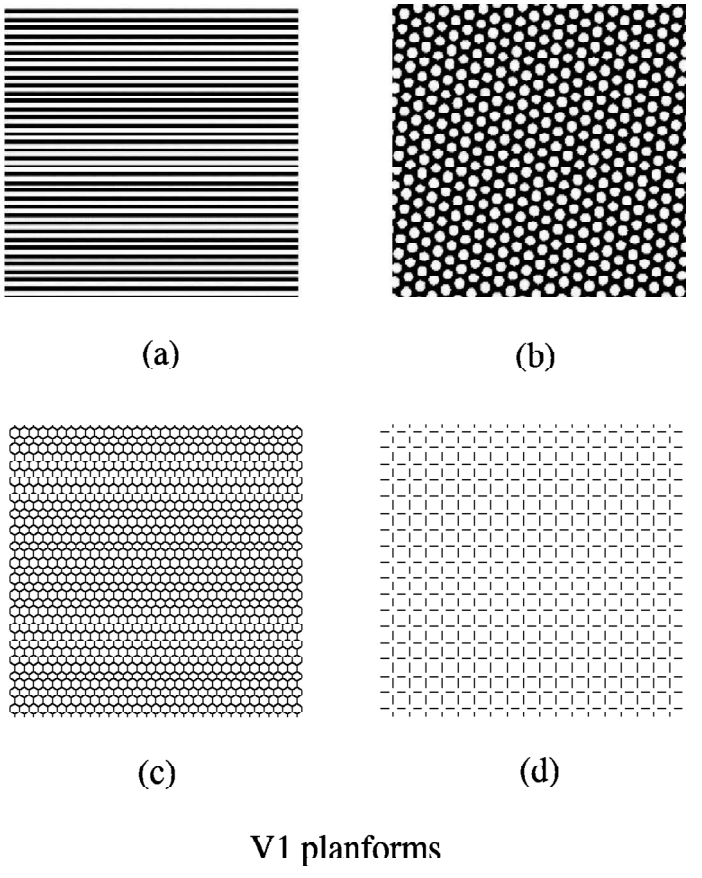

Figure 5: V1 Planforms corresponding to some axial subgroups. (a, b): Roll and hexagonal patterns generated in V1 when it is in the Hubel-Wiesel operating mode. (c, d) Honeycomb and square patterns generated when V1 is in the coupled-ring operating mode.

3.1 Form Constants as Stable Planforms. Figure 5 shows some of the (mostly) stable planforms defined above in V1 coordinates and Figure 6 in visual field coordinates, generated by plotting at each point $\mathbf{r}$ a contour element at the orientation ϕ most strongly signaled at that point—that point,that is, for which $a(\mathbf{r}, \phi)$ is largest.

These planforms are either contoured or noncontoured and correspond closely to Kluver's form constants. In what we call the Hubel-Wiesel mode, interactions between iso-orientation patches in a single hypercolumn are weak and purely excitatory, so individual hypercolumns do not amplify any particular orientation. However, if the long-range interactions are stronger

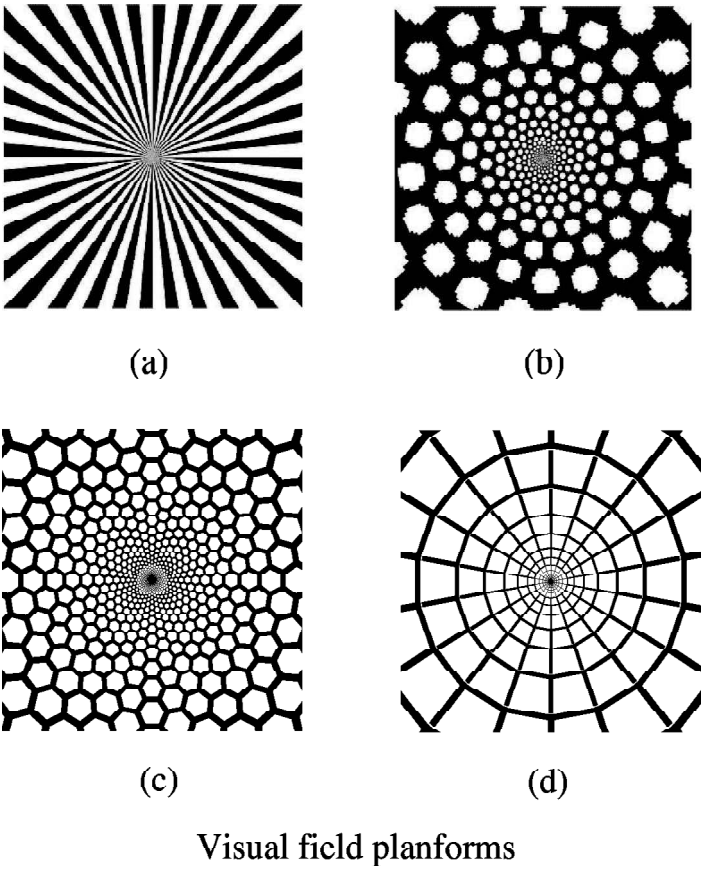

Figure 6: The same planforms as shown in Figure 5 drawn in visual field coordinates. Note however, that the feathering around the edges of the bright blobs in *b* is a fortuitous numerical artifact.

and effectively inhibitory, then plane waves of cortical activity can emerge, with no label for orientation preference. The resulting planforms are called noncontoured and correspond to the types I and II form constants, as originally proposed by Ermentrout and Cowan (1979). On the other hand, if coupled-ring-mode interactions between neighboring iso-orientation patches are strong enough so that even weakly biased activity can trigger a sharply tuned response, under the combined action of many interacting hypercolumns, plane waves labeled for orientation preference can emerge. The resulting planforms correspond to types III and IV form constants. These results suggest that the circuits in V1 that are normally involved in the detection of oriented edges and the formation of contours are also responsible

for the generation of the form constants. Since 20% of the (excitatory) lateral connections in layers 2 and 3 of V1 end on inhibitory interneurons (Hirsch & Gilbert, 1991), the overall action of the lateral connections can become inhibitory, especially at high levels of activity. The mathematical consequence of this inhibition is the selection of odd planforms that do not form continuous contours. We have shown that even planforms that do form continuous contours can be selected when the overall action of the lateral connection is inhibitory, if the model assumes deviation away from the visuotopic axis by at least 45 degrees in the pattern of lateral connections (Bressloff et al., 2001) (as opposed to our first model, in which connections between iso-orientation patches are oriented along the visuotopic axis).

This might seem paradoxical given observations suggesting that there are at least two circuits in V1: one dealing with contrast edges, in which the relevant lateral connections have the anisotropy found by Bosking et al. (1997), and others that might be involved with the processing of textures, surfaces, and color contrast, which seem to have a much more isotropic lateral connectivity (Livingstone & Hubel, 1984). However, there are several intriguing possibilities that make the analysis more plausible. The first can occur in case V1 operates in the Hubel-Wiesel mode ($p_c = 0$). In such an operating mode, if the lateral interactions are not as weak as we have assumed in our analysis, then even contoured planforms can form. The second related possibility can occur if at low levels of activity, V1 operates initially in the Hubel-Wiesel mode and the lateral and long-range interactions are all excitatory ($p_c = q_c = 0$), so that a bulk instability occurs if the homogeneous state becomes unstable, which can be followed by the emergence of patterned noncontoured planforms at the critical wavelength of about 2.67 mm, when the level of activity rises, and the longer-ranged inhibition is activated ($p_c = 0, q_c \neq 0$), until V1 operates in the coupled-ring mode when the short-range inhibition is also activated ($p_c \neq 0$, $q_c \neq 0$). In such a case, even planforms can be selected by the anistropic connectivity, since the degeneracy has already been broken by the noncontoured planforms. A third possibility is related to an important gap in our current model: we have not properly incorporated the observation that the distribution of orientation preferences in V1 is not spatially homogeneous. In fact, the well-known orientation "pinwheel" singularities originally found by Blasdel and Salama (1986) turn out to be regions in which the scatter or rate of change $|\Delta\phi/\Delta\mathbf{r}|$ of differing orientation preference labels is high—about 20 degrees—whereas in linear regions, it is only about 10 degrees (Maldonado & Gray, 1996). Such a difference leads to a second model circuit (centered on the orientation pinwheels) with a lateral patchy connectivity that is effectively isotropic (Yan, Dimitrov, & Cowan, 2001) and therefore consistent with observations of the connectivity of pinwheel regions (Livingstone & Hubel, 1984). In such a case, even planforms are selected in the coupled-ring mode. Types I and II noncontoured form constants could also arise from a "filling-in" process similar to that embodied in the retinex algo-

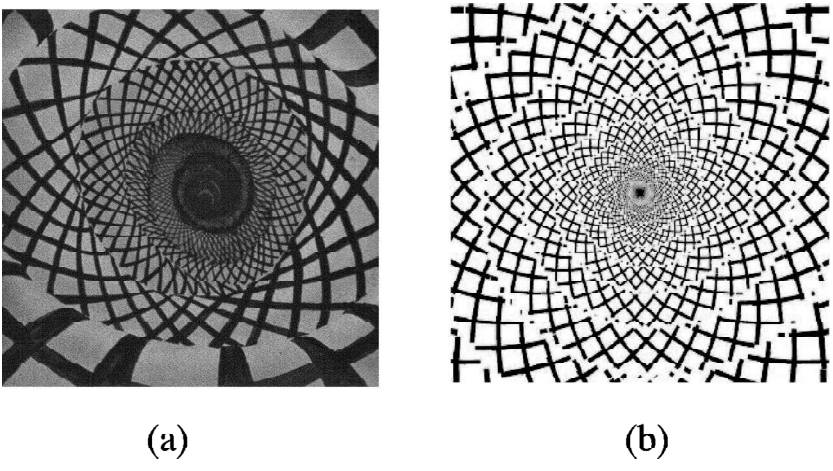

Figure 7: (a) Lattice tunnel hallucination seen following the taking of marijuana (redrawn from Siegel & Jarvik, 1975), with the permission of Alan D. Iselin. (b) Simulation of the lattice tunnel generated by an even hexagonal roll pattern on a square lattice.

rithm of Land and McCann (1971) following the generation of types III or IV form constants in the coupled-ring mode. The model allows for oscillating or propagating waves, as well as stationary patterns, to arise from a bulk instability. Such waves are in fact observed: many subjects who have taken LSD and similar hallucinogens report seeing bright white light at the center of the visual field, which then "explodes" into a hallucinatory image (Siegel, 1977) in at most 3 seconds, corresponding to a propagation velocity in V1 of about 2.5 cm per second, suggestive of slowly moving epileptiform activity (Senseman, 1999). In this respect, it is worth noting that in the continuum approximation we use in this study, both planforms arising when the long-range interactions are purely excitatory correspond to the perception of a uniform bright white light.

Finally, it should be emphasized that many variants of the Klüver form constants have been described, some of which cannot be understood in terms of the model we have introduced. For example the lattice tunnel shown in Figure 7a is more complicated than any of the simple form constants shown earlier. One intriguing possibility is that this image is generated as a result of a mismatch between the corresponding planform and the underlying structure of V1. We have (implicitly) assumed that V1 has patchy connections that endow it with lattice properties. It is clear from the optical image data (Blasdel & Salama, 1986; Bosking et al., 1997) that the cortical lattice is somewhat disordered. Thus, one might expect some distortions to occur when planforms are spontaneously generated in such

a lattice. Figure 7b shows a computation of the appearance in the visual field of a roll pattern on a hexagonal lattice represented on a square lattice, so that there is a slight incommensurability between the two. The resulting pattern matches the hallucinatory image shown in Figure 7a quite well.

4 Discussion

This work extends previous work on the cortical mechanisms underlying visual hallucinations (Ermentrout & Cowan, 1979) by explicitly considering cells with differing orientation preferences and by considering the action of the retino-cortical map on oriented edges and local contours. This is carried out by the tangent map associated with the complex logarithm, one consequence of which is that ϕ, the V1 label for orientation preference, is not exactly equal to orientation preference in the visual field, ϕ_R but differs from it by the angle θ_R, the polar angle of receptive field position. It follows that elements tuned to the same angle ϕ should be connected along lines at that angle in V1. This is consistent with the observations of Blasdel and Sincich (personal communication, 1999) and Bosking et al. (1997) and with one of Mitchison and Crick's (1982) hypotheses on the lateral connectivity of V1. Note that near the vertical meridian (where most of the observations have been made), changes in ϕ approximate closely changes in ϕ_R. However, such changes should be relatively large and detectable with optical imaging near the horizontal meridian.

Another major feature outlined in this article is the presumed Euclidean symmetry of V1. Many systems exhibit Euclidean symmetry. What is novel here is the way in which such a symmetry is generated: by a shift $\{\mathbf{r}, \phi\} \to \{\mathbf{r} + \mathbf{s}, \phi\}$ followed by a twist $\{\mathbf{r}, \phi\} \to \{R_\theta[\mathbf{r}], \phi + \theta\}$, as well as by the usual translations and reflections. It is the twist $\phi \to \phi + \theta$ that is novel and is required to match the observations of Bosking et al. (1997). In this respect, it is interesting that Zweck and Williams (2001) recently introduced a set of basis functions with the same shift-twist symmetry as part of an algorithm to implement contour completion. Their reason for doing so is to bind sparsely distributed receptive fields together functionally, so as to perform Euclidean invariant computations. It remains to explain the precise relationship between the Euclidean invariant circuits we have introduced here and Euclidean invariant receptive field models.

Finally, we note that our analysis indicates the possibility that V1 can operate in two different dynamical modes, the Hubel-Wiesel mode or the coupled-ring mode, depending on the levels of excitability of its various excitatory and inhibitory cell populations. We have shown that the Hubel-Wiesel mode can spontaneously generate noncontoured planforms and the coupled-ring mode contoured ones. Such planforms are seen as hallucinatory images in the visual field, and their geometry is a direct consequence of the architecture of V1. We conjecture that the ability of V1 to process edges,

contours, surfaces, and textures is closely related to the existence of these two modes.

Acknowledgments

We thank A. G. Dimitrov, T. Mundel, and G. Blasdel and the referees for many helpful discussions. The work was supported by the Leverhulme Trust (P.C.B.), the James S. McDonnell Foundation (J.D.C.), and the National Science Foundation (M.G.). P. C. B. thanks the Mathematics Department, University of Chicago, for its hospitality and support. M. G. thanks the Center for Biodynamics, Boston University, for its hospitality and support. J. D. C. and P. C. B. thank G. Hinton and the Gatsby Computational Neurosciences Unit, University College, London, for hospitality and support.

References

Blackmore, S. J. (1992). *Beyond the body: An investigation of out–of–the–body experiences*. Chicago: Academy of Chicago.

Blasdel, G., & Salama, G. (1986). Voltage-sensitive dyes reveal a modular organization in monkey striate cortex. *Nature, 321*(6070), 579–585.

Bosking, W. H., Zhang, Y., Schofield, B., & Fitzpatrick, D. (1997). Orientation selectivity and the arrangemen t of horizontal connections in tree shrew striate cortex. *J. Neurosci., 17*, 2112–2127.

Bressloff, P. C., Cowan, J. D., Golubitsky, M., Thomas, P. J., & Wiener, M. C. (2001). Geometric visual hallucinations, Euclidean symmetry, and the functional architecture of striate cortex. *Phil. Trans. Roy Soc. Lond. B, 356*, 299–330.

Clottes, J., & Lewis-Williams, D. (1998). *The shamans of prehistory: Trance and magic in the painted caves*. New York: Abrams.

Collier, B. B. (1972). Ketamine and the conscious mind. *Anaesthesia, 27*, 120–134.

Cowan, J. D. (1977). Some remarks on channel bandwidths for visual contrast detection. *Neurosciences Research Program Bull., 15*, 492–517.

Cowan, J. D. (1997). Neurodynamics and brain mechanisms. In M. Ito, Y. Miyashita, & E. T. Rolls (Eds.), *Cognition, computation, and consciousness* (pp. 205–233). New York: Oxford University Press.

Drasdo, N. (1977). The neural representation of visual space. *Nature, 266*, 554–556.

Dybowski, M. (1939). Conditions for the appearance of hypnagogic visions. *Kwart. Psychol., 11*, 68–94.

Ermentrout, G. B. (1998). Neural networks as spatial pattern forming systems. *Rep. Prog. Phys., 61*, 353–430.

Ermentrout, G. B., & Cowan, J. D. (1979). A mathematical theory of visual hallucination patterns. *Biol. Cybernetics, 34*, 137–150.

Gilbert, C. D., & Wiesel, T. N. (1983). Clustered intrinsic connections in cat visual cortex. *J. Neurosci., 3*, 1116–1133.

Golubitsky, M., & Schaeffer, D. G. (1985). *Singularities and groups in bifurcation theory I*. Berlin: Springer-Verlag.

Golubitsky, M., Stewart, I., & Schaeffer, D. G. (1988). *Singularities and groups in bifurcation theory II*. Berlin: Springer-Verlag.

Hansel, D., & Sompolinsky, H. (1997). Modeling feature selectivity in local cortical circuits. In C. Koch & I. Segev (Eds.), *Methods of neuronal modeling* (2nd ed., pp. 499–567). Cambridge, MA: MIT Press.

Helmholtz, H. (1925). *Physiological optics* (Vol. 2). Rochester, NY: Optical Society of America.

Hirsch, J. D., & Gilbert, C. D. (1991). Synaptic physiology of horizontal connections in the cat's visual cortex. *J. Neurosci., 11*, 1800–1809.

Horton, J. C., & Hedley-Whyte, E. T. (1984). Mapping of cytochrome oxidase patches and ocular dominance columns in human visual cortex. *Phil. Trans. Roy. Soc. B, 304*, 255–272.

Hubel, D. H., & Wiesel, T. N. (1962). Receptive fields, binocular interaction and functional architecture in the cat's visual cortex. *J. Physiol. (Lond.), 160*, 106–154.

Hubel, D. H., & Wiesel, T. N. (1974). Sequence regularity and geometry of orientation columns in the monkey striate cortex. *J. Comp. Neurol., 158*, 267–294.

Klüver, H. (1966). *Mescal and mechanisms of hallucinations*. Chicago: University of Chicago Press.

Land, E., & McCann, J. (1971). Lightness and retinex theory. *J. Opt. Soc. Am., 61*(1), 1–11.

Levitt, J. B., Lund, J., & Yoshioka, T. (1996). Anatomical substrates for early stages in cortical processing of visual information in the macaque monkey. *Behavioral Brain Res., 76*, 5–19.

Livingstone, M. S., & Hubel, D. H. (1984). Specificity of intrinsic connections in primate primary visual cortex. *J. Neurosci., 4*, 2830–2835.

Maldonado, P., & Gray, C. (1996). Heterogeneity in local distributions of orientation-selective neurons in the cat primary visual cortex. *Visual Neuroscience, 13*, 509–516.

Mavromatis, A. (1987). *Hypnagogia: The unique state of consciousness between wakefulness and sleep*. London: Routledge & Kegan Paul.

Mitchison, G., & Crick, F. (1982). Long axons within the striate cortex: Their distribution, orientation, and patterns of connection. *Proc. Nat. Acad. Sci. (USA), 79*, 3661–3665.

Miyashita, Y. (1995). How the brain creates imagery: Projection to primary visual cortex. *Science, 268*, 1719–1720.

Mundel, T., Dimitrov, A., & Cowan, J. D. (1997). Visual cortex circuitry and orientation tuning. In M. C. Mozer, M. I. Jordan, & T. Petsche (Eds.), *Advances in neural information processing systems, 9* (pp. 887–893). Cambridge, MA: MIT Press.

Patterson, A. (1992). *Rock art symbols of the greater southwest*. Boulder, CO: Johnson Books.

Purkinje, J. E. (1918). *Opera omnia* (Vol. 1). Prague: Society of Czech Physicians.

Schwartz, E. (1977). Spatial mapping in the primate sensory projection: Analytic structure and relevance to projection. *Biol. Cybernetics, 25*, 181–194.

Senseman, D. M. (1999). Spatiotemporal structure of depolarization spread in cortical pyramidal cell populations evoked by diffuse retinal light flashes. *Visual Neuroscience, 16*, 65–79.

Sereno, M. I., Dale, A. M., Reppas, J. B., Kwong, K. K., Belliveau, J. W., Brady, T. J., Rosen, B. R., & Tootell, R. B. H. (1995). Borders of multiple visual areas in humans revealed by functional magnetic resonance imaging. *Science, 268*, 889–893.

Siegel, R. K. (1977). Hallucinations. *Scientific American, 237*(4), 132–140.

Siegel, R. K., & Jarvik, M. E. (1975). Drug–induced hallucinations in animals and man. In R. K. Siegel & L. J. West (Eds.), *Hallucinations: Behavior, experience and theory* (pp. 81–161). New York: Wiley.

Smythies, J. R. (1960). The stroboscopic patterns III. further experiments and discussion. *Brit. J. Psychol., 51*(3), 247–255.

Somers, D., Nelson, S., & Sur, M. (1996). An emergent model of orientation selectivity in cat visual cortex simple cells. *J. Neurosci., 15*(8), 5448–5465.

Turing, A. M. (1952). The chemical basis of morphogenesis. *Phil. Trans. Roy Soc. Lond. B, 237*, 32–72.

Tyler, C. W. (1978). Some new entoptic phenomena. *Vision Res., 181*, 1633–1639.

Tyler, C. W. (1982). Do grating stimuli interact with the hypercolumn spacing in the cortex? *Suppl. Invest. Ophthalmol., 222*, 254.

Walgraef, D. (1997). *Spatio–temporal pattern formation*. New York: Springer-Verlag.

Wiener, M. C. (1994). *Hallucinations, symmetry, and the structure of primary visual cortex: A bifurcation theory approach*. Unpublished doctoral dissertation, University of Chicago.

Wilson, H. R., & Cowan, J. D. (1973). A mathematical theory of the functional dynamics of cortical and thalamic nervous tissue. *Kybernetik, 13*, 55–80.

Yan, C.-P., Dimitrov, A., & Cowan, J. (2001). *Spatial inhomogeneity in the visual cortex and the statistics of natural images*. Unpublished manuscript.

Zubek, J. (1969). *Sensory deprivation: Fifteen years of research*. New York: Appleton-Century-Crofts.

Zweck, J. W., & Williams, L. R. (2001). *Euclidean group invariant computation of stochastic completion fields using shiftable-twistable functions*. Manuscript submitted for publication.

Received December 20, 2000; accepted April 26, 2001.